



# Preparation of UiO-66-NH<sub>2</sub>@cellulose nanofiber composite film and its adsorption performance study towards Cd(II)

Hao He<sup>1,2</sup> · Xiao-kai Liu<sup>1,2</sup> · Bai-yun Zhao<sup>1,2,3</sup> · Li-juan Zhou<sup>1,2,3</sup> · Xuan Zhao<sup>1,2,3</sup> · Chen-xu Wang<sup>1,2,3</sup> · Li Wang<sup>1,2,3</sup>

Received: 21 March 2024 / Revised: 30 May 2024 / Accepted: 10 June 2024

© The Author(s), under exclusive licence to Springer-Verlag GmbH Germany, part of Springer Nature 2024

## Abstract

A novel heavy metal ion adsorbent, UiO-66-NH<sub>2</sub>@cellulose nanofiber membrane, was successfully synthesized using cellulose and polyvinyl alcohol as substrates and UiO-66-NH<sub>2</sub> as the loading material. The adsorption performance of the composite membrane towards Cd(II) was investigated through adsorption experiments. The adsorption results showed that under the optimal adsorption conditions (temperature of 45 °C, adsorption time of 2 h, and Cd(II) solution pH of 0.89), the maximum adsorption capacity was 611.89 mg·g<sup>-1</sup> with cellulose, UiO-66-NH<sub>2</sub>, and PVA added at 0.8 g, 0.15 g, and 1.2 g, respectively. Subsequently, the structure of the composite membrane was characterized using SEM, FT-IR, and XPS, and the adsorption mechanism was preliminarily explored by combining adsorption kinetics and isotherms. The results indicated the formation of a complex three-dimensional network structure during the crosslinking of cellulose and polyvinyl alcohol, with UiO-66-NH<sub>2</sub> loaded on the surface and internal pores of the network structure. Furthermore, FT-IR and XPS spectra showed the formation of coordination bonds between the composite membrane and Cd(II) through -OH, -NH<sub>2</sub>, and Zr-O and the confirmation of a negative surface charge on the composite membrane through isoelectric point testing, indicating the significant role of electrostatic interactions in Cd(II) adsorption. Adsorption kinetics and isotherm results indicated that the adsorption process was primarily complex multilayer chemisorption. In summary, the adsorption of Cd(II) by UiO-66-NH<sub>2</sub>@cellulose nanofiber membrane involves coordination between metal ions and NO, as well as pore filling and electrostatic adsorption.

**Keywords** UiO-66-NH<sub>2</sub> · Cellulose · Adsorption · Cd(II) · Nanofiber membrane

## 1 Introduction

With the continuous development of industrialization, environmental pollution issues have become increasingly prominent, among which heavy metal pollution is one of the most serious environmental issues, with Cd(II) ranking at the forefront of heavy metal pollution. A large amount of Cd

is discharged into the environment through exhaust gases, wastewater, and waste residues, causing serious pollution. Cd pollution manifests in two forms: gaseous and aqueous. Gaseous pollution mainly originates from industrial exhaust gases, with cadmium spreading with the gases to the surroundings of factories and naturally settling, accumulating in the surrounding soil. Aqueous pollution is mainly caused by the discharge of wastewater from lead–zinc ore dressing and related industries (such as electroplating and alkaline batteries) into surface water or seeping into groundwater. With the accumulation of Cd in soil and water bodies, cadmium accumulates in organisms, entering the human body through the food chain, directly affecting human life [1]. When Cd enters the human body through the respiratory and digestive tracts, it forms cadmium-metallothionein complexes in the body, circulating throughout the body via the bloodstream and selectively accumulating in the kidneys and liver. Additionally, there is a certain accumulation in the spleen, pancreas, thyroid, testes, and hair. When the internal content is excessive, it can lead to bone disorders, liver

---

Hao He and Xiao-Kai Liu contributed equally to this work.

✉ Li Wang  
wldcl@126.com

<sup>1</sup> School of Materials Science and Art and Design, Inner Mongolia Agricultural University, Hohhot 010018, China

<sup>2</sup> Laboratory of Fibrosis and Energy Utilization of Shrubby Resources in Inner Mongolia Autonomous Region, Hohhot, China

<sup>3</sup> National Forestry Grassland Engineering Technology Research Center for Efficient Development and Utilization of Sandy Shrubs, Hohhot, China

damage, cardiovascular diseases, and sexual dysfunction and disrupt the mineral balance in the body [2]. Therefore, the environmental pollution problem caused by Cd urgently needs to be addressed.

At present, the methods of removing heavy metal ion pollutants mainly include precipitation method, electrochemical method, adsorption separation method, membrane separation method, ion exchange method, physical and chemical method and biological method (biological flocculation method, biological adsorption method, plant remediation method) [3–8]. Among them, the adsorption separation method is relatively simple, and there are many kinds of adsorbents, which is the most commonly used method. Common materials such as carbonaceous materials, metal organic framework materials, mineral materials, and biomass materials, for environmentally friendly biocompatible biodegradable, low toxicity and renewable heavy metal adsorption materials have become a research hotspot.

Metal–organic framework (MOF) is a crystal structure synthesized by organic linkers and inorganic metal ions or metal clusters. Due to its large surface area, high porosity, and good stability, it has been widely used in gas separation, energy conversion, catalysis, sensing, organic degradation, metal ion adsorption and biomedical applications [9–11]. UiO-66-NH<sub>2</sub> is a metal–organic framework material developed with Zr<sup>4+</sup> as the metal center and 2-aminoterephthalic acid as the ligand. It has strong thermal stability and chemical stability, and the porosity of UiO-66-NH<sub>2</sub> is large. The introduction of amino groups will make it more excellent in some aspects [12–14] and easier to be functionalized. Therefore, the function of UiO-66-NH<sub>2</sub> as an excellent heavy metal ion adsorbent in removing pollutants from aqueous solution has received extensive attention. Due to the crystallinity of the material itself, it mostly exists in the form of powder and is prone to agglomeration in water, and it is easy to cause pipeline blockage in the adsorption system [15], which is not conducive to recycling. Therefore, the combination of UiO-66-NH<sub>2</sub> with appropriate substrate materials is an effective method to realize its functional recovery and reuse [16]. Zhang et al. [17] successfully fabricated a PEI/metal–organic framework@polyvinylidene fluoride (PEI/MOF@PVDF) composite membrane by depositing UiO-66-NH<sub>2</sub> and cross-linking it with PVDF and PEI. The composite membrane demonstrated an effective treatment volume of 2322.23 L·m<sup>-2</sup> for Cr (VI) through electrostatic attraction, while Cr(III) maintained a stable effluent concentration of 10.4 mg·L<sup>-1</sup> via the Donnan effect. Furthermore, the effective treatment volume of the composite membrane remained above 91.83% after three cycles, making it an ideal adsorbent material.

Cellulose nanofiber is an essential component of biomass, being the most abundant natural polymer material on Earth. Its stable physicochemical properties, non-toxicity,

biodegradability, and low cost make cellulose materials representative of economically and environmentally friendly materials. Additionally, due to its abundant hydroxyl groups on the surface, cellulose nanofiber is widely used in the field of heavy metal ion adsorption [18].

Therefore, to address the issues of pipeline blockage and difficult recovery of UiO-66-NH<sub>2</sub> in aqueous environments, UiO-66-NH<sub>2</sub> was loaded onto cellulose nanofiber membranes (UNC) using cellulose as the substrate and an ionic liquid ([AMIM]Cl) as the solvent via wet spinning. The optimal preparation conditions of the composite membrane were investigated by varying the amounts of cellulose, PVA, and UiO-66-NH<sub>2</sub>. The optimal adsorption conditions of UNC for Cd(II) were determined by altering the initial concentration and pH of the Cd(II) solution, as well as the adsorption temperature and time. The materials were characterized using SEM, FT-IR, XRD, and XPS to explore the microstructural changes during processing, and the adsorption mechanism was preliminarily elucidated by combining adsorption kinetics and isotherm studies. This method offers shorter adsorption time, lower usage, and reduced costs for treating Cd(II) wastewater, while also addressing issues of UiO-66-NH<sub>2</sub> aggregation and pipeline blockage during adsorption, providing valuable insights for the application of MOF materials and Cd(II) wastewater treatment.

## 2 Experiment part

### 2.1 Experimental materials and instruments

Tables 1 and 2 are the materials and instruments required for the experiment.

### 2.2 Synthesis of the UiO-66-NH<sub>2</sub>

UiO-66-NH<sub>2</sub> was synthesized by an improved solvothermal method [19]. Then, 0.4 g of 2-aminoterephthalic acid and 0.5 g of ZrCl<sub>4</sub> were added to 30 mL of DMF and ultrasonically dissolved to form a solution. The solution was then poured into a hydrothermal reactor and reacted at 120 °C for 12 h. After that, the solution after the reaction was filtered, and the yellow solid was obtained by washing with DMF and methanol for many times. The yellow solid was dried in an oven at 60 °C for 12 h to get a yellow powder UiO-66-NH<sub>2</sub>.

### 2.3 Preparation of the UNC

A certain capacity of cellulose (0.4 g, 0.8 g, 1.2 g, 1.6 g, and 2.0 g) was dissolved in 15 g dimethyl sulfoxide and 4 g ionic liquid and stirred in a water bath at 85 °C for 4 h. Then, an appropriate capacity of UiO-66-NH<sub>2</sub> (0.05 g, 0.1 g, 0.15 g, 0.2 g, and 0.25 g) was added to continue

**Table 1** Experimental materials

Experiment reagent	Reagent grade	Manufacturer
Cellulose	AR	Hebei Bailingwei Ultrafine Materials Co., Ltd
Zirconium chloride (ZrCl <sub>4</sub> )	AR	Shanghai Aladdin Biochemical Technology Co., Ltd
Ionic liquid ([AMIM]Cl)	AR	Shenyang Sinos Technology Co., Ltd
N,N-Dimethylformamide	AR	Fu Chen (Tianjin) Chemical Reagent Co., Ltd
2-Aminoterephthalic acid	AR	Shanghai Aladdin Biochemical Technology Co., Ltd
Polyvinyl alcohol (PVA)	AR	Chemical Reagent Co., Ltd
Dimethyl sulfoxide (DMSO)	AR	Fu Chen (Tianjin) Chemical Reagent Co., Ltd
Ethanol	AR	Tianjin Guangfu Technology Development Co., Ltd

**Table 2** Experimental instruments

Laboratory apparatus	Model	Manufacturer
Drying vacuum oven	DZF-6210	Shanghai Shanzhi Instrument and Equipment Co., Ltd
pH measuring instrument	STARTER3100	Ohaus Instruments Shanghai Co., Ltd
Dual-beam ultraviolet–visible spectrophotometer	TU-1901	Beijing Persee General Instrument Co., Ltd
Infrared spectrometer	SOR-27	Bruker Optics, Germany
X-ray diffractometer	D8ADVANCE	Bruker Optics, Germany
Scanning electron microscope	6701F	JSM Company, Japan
Hydrothermal reactor	YSKH	Shanghai Shenke Instrument Co., Ltd

stirring for 1 h, and then, a certain capacity of PVA (0.6 g, 0.8 g, 1.0 g, 1.2 g, and 1.4 g) was added to stir for 1.5 h. The spinning solution was prepared and the primary filament was obtained. UNC was prepared by soaking in anhydrous ethanol for 2 h in coagulation bath and drying in a vacuum oven at 50 °C for 12 h.

## 2.4 Cd(II) adsorption experiments

50 mL Cd(II) solution with a certain concentration (600 mg·L<sup>-1</sup>, 700 mg·L<sup>-1</sup>, 800 mg·L<sup>-1</sup>, 900 mg·L<sup>-1</sup>, and 1000 mg·L<sup>-1</sup>) was added to the conical flask, and then, 0.05 g UNC was added. The solution was placed in a constant temperature water bath oscillation box at different temperatures (25 °C, 35 °C, 45 °C, 55 °C, and 65 °C). At different pH values (0.89, 2, 3, 4, and 5), adsorption time (1 h, 2 h, 3 h, 4 h, and 5 h). After the adsorption experiment, the concentration of Cd(II) in the water after adsorption was measured by ultraviolet spectrophotometer at 600 nm. Substituted into the formula (1), the adsorption capacity of UNC to Cd(II) was calculated.

$$Q_e = (C_0 - C_e) \times V/m \quad (1)$$

$Q_e$  is the capacity of adsorption (mg·g<sup>-1</sup>),  $C_0$  is the Cd(II) concentration before adsorption (mg·L<sup>-1</sup>),  $C_e$  is the Cd(II) concentration after adsorption (mg·L<sup>-1</sup>),  $V$  is the volume of Cd(II) solution (L), and  $m$  is the mass of adsorbent (g).

## 2.5 Characterization

### 2.5.1 SEM characterization

The microstructure of the samples was analyzed by scanning electron microscopy. The conductive adhesive is attached to the sample, and an appropriate capacity of sample is taken on the conductive adhesive. The unfixed sample is cleaned, and then, the sample is dried and sprayed with gold. The acceleration current is 5 kV, and the appropriate magnification is observed.

### 2.5.2 FTIR characterization

The Fourier transform infrared spectrometer was used to analyze the infrared spectrum of the sample. The sample was subjected to KBr tableting, with a resolution of 4 cm<sup>-1</sup> and a wavenumber range of 450~4000 cm<sup>-1</sup>. The ZnSe prism and 60° incident angle were used, and the number of scans was 160 times.

### 2.5.3 XRD characterization

The samples were analyzed by XRD. The samples were placed on a blank glass slide, compacted and sent to the sample chamber. The incident wavelength was 0.514 nm,

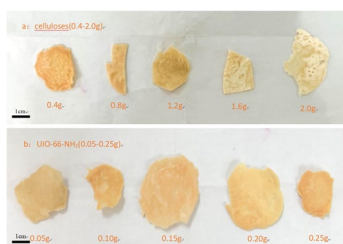


**Fig. 1** UNC (a) with different cellulose dosage and UNC (b) with different UiO-66-NH<sub>2</sub> dosage

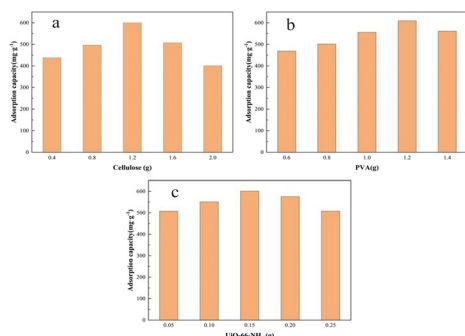


**Fig. 2** Effects of **a** the amount of cellulose addition, **b** the amount of PVA addition, and **c** the amount of UiO-66-NH<sub>2</sub> addition on the adsorption capacity of Cd(II)

the scanning range was 10–90°, the scanning speed was 4 (°)/min, and the scanning interval was 0.02°.

### 2.5.4 XPS characterization

The surface elements and their valence states of the samples were analyzed by X-ray photoelectron spectroscopy. The Al target Ka ray was used as the laser source, the photoelectron energy was 1486.6 eV, and the electron binding energy was corrected using the 284.6 eV of C1s as the reference. The characteristic peak error was  $\pm 0.47$  eV.

## 3 Result and discussion

### 3.1 Preparation experiments

Figure 1 shows images of UNC composite membranes with (a) different cellulose contents and (b) different UiO-66-NH<sub>2</sub> contents.

#### 3.1.1 Dosage of cellulose

When the dosage of PVA is 1.2 g and the dosage of UiO-66-NH<sub>2</sub> is 0.15 g, the effect of the dosage of cellulose on the adsorption of Cd(II) by UNC is shown in Fig. 2a. From

Fig. 2a, it can be seen that as the dosage of cellulose gradually increases, the adsorption capacity of UNC to Cd(II) increases first and then decreases. When the dosage of cellulose is 0.8 g, the adsorption capacity of UNC to Cd(II) reaches the maximum, which is 599.72 mg·g<sup>-1</sup>. This may be due to the fact that cellulose is used as the substrate material to accommodate UiO-66-NH<sub>2</sub>. When the dosage is insufficient, UiO-66-NH<sub>2</sub> cannot be completely evenly distributed in it. It can be seen from Fig. 1a that when the dosage of cellulose is small, UiO-66-NH<sub>2</sub> agglomerates and accumulates, and UNC shows dark yellow. With the increase of cellulose dosage, the color gradually becomes lighter, which indicates that UiO-66-NH<sub>2</sub> is gradually uniformly dispersed in it. However, when the capacity of cellulose is too much, UiO-66-NH<sub>2</sub> is too dispersed in it. The content of UiO-66-NH<sub>2</sub> in UNC with the same mass decreased sharply, and the adsorption capacity decreased. Therefore, the optimum dosage of cellulose was 0.8 g.

#### 3.1.2 Dosage of PVA

When the dosage of cellulose was 0.8 g and the dosage of UiO-66-NH<sub>2</sub> was 0.15 g, the effect of PVA dosage on the adsorption of Cd(II) by UNC was shown in Fig. 2b. It can be seen from Fig. 2b that with the increase of PVA dosage, the adsorption capacity of UNC to Cd(II) increased first and then decreased. When the dosage of cellulose was 1.2 g, the adsorption capacity of UNC to Cd(II) reached the maximum, which was 609.11 mg·g<sup>-1</sup>. It can be seen from the SEM characterization results that the dissolved cellulose PVA was crosslinked to form a three-dimensional network structure [20], and UiO-66-NH<sub>2</sub> was uniformly attached to the three-dimensional network structure. When the dosage of PVA is less, it cannot be well crosslinked with the dissolved cellulose, so that the adsorption capacity is low. When the dosage of PVA increased, it was too tightly crosslinked with cellulose, so that the UiO-66-NH<sub>2</sub> was tightly wrapped, some adsorption sites could not be exposed, and the adsorption capacity decreased. Therefore, the optimum dosage of PVA is 1.2 g.

#### 3.1.3 Dosage of UiO-66-NH<sub>2</sub>

When the dosage of PVA was 1.2 g and the dosage of cellulose was 0.8 g, the effect of the dosage of UiO-66-NH<sub>2</sub> on the adsorption of Cd(II) by UNC was shown in Fig. 2c. It can be seen from Fig. 2c that with the increase of the dosage of UiO-66-NH<sub>2</sub>, the adsorption capacity of UNC to Cd(II) increased first and then decreased. When the dosage of cellulose was 0.15 g, the adsorption capacity of UNC to Cd(II) reached the maximum, which was 601.08 mg·g<sup>-1</sup>. From Fig. 1b, it can be seen that as the dosage of UiO-66-NH<sub>2</sub> gradually increases, the color deepens from light yellow to

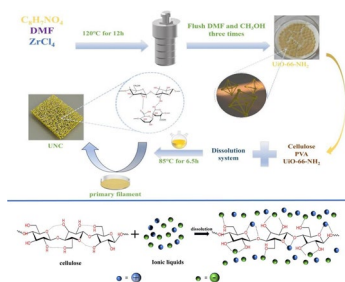


**Fig. 3** Preparation process and internal structure of UNC

dark yellow, indicating that the content of UiO-66-NH<sub>2</sub> in UNC per unit weight gradually increases, and the number of adsorption sites and active functional groups [21] also increases, so the adsorption capacity gradually increases. However, when the content of UiO-66-NH<sub>2</sub> is too high, it can be seen from the SEM photos that UiO-66-NH<sub>2</sub> is agglomerated and accumulated in the three-dimensional network structure, which makes the adsorption sites gradually decrease and the adsorption capacity decrease. Therefore, the optimal dosage of UiO-66-NH<sub>2</sub> is 0.15 g.

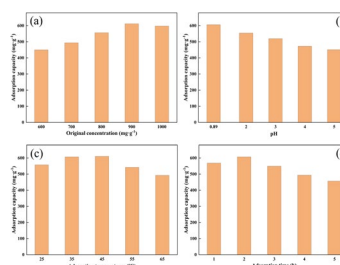
### 3.1.4 Preparation mechanism

Figure 3 illustrates the formation process of the UNC composite membrane and the dissolution process of cellulose. Under the action of ionic liquids, the synergy of anions and cations disrupts the hydrogen bonds of cellulose, gradually dissolving cellulose and cross-linking with PVA to form a three-dimensional network structure. With the passage of time, the ionic liquid in the membrane begins to precipitate, and this precipitation process forms an excellent pore structure, which is conducive to the distribution of UiO-66-NH<sub>2</sub> within it. The interaction between cellulose and PVA generates hydrogen bonds, which enhance the stability of the structure.

## 3.2 Adsorption experiment

### 3.2.1 Initial concentration of Cd(II) solution

When the adsorption time was 2 h, the adsorption temperature was 45 °C, and the pH was 0.89, the effect of the initial concentration of Cd(II) solution on the adsorption of Cd(II) by UNC was shown in Fig. 4a. It can be seen from Fig. 4a that with the increase of Cd(II) solution concentration, the adsorption capacity of UNC to Cd(II) increased first and then decreased slightly. When the concentration of Cd(II) solution was 900 mg·L<sup>-1</sup>, the adsorption capacity of UNC to Cd(II) reached the maximum, which was 611.89 mg·g<sup>-1</sup>. In the early stage of adsorption, the diffusion rate of Cd(II) was accelerated due to the increase of



**Fig. 4** Effects of four adsorption conditions: **a** the initial concentration of Cd(II) solution and adsorption temperature, **b** the pH value of the Cd(II) solution, **c** adsorption temperature, and **d** adsorption time

concentration difference driving force, which increased the probability of Cd(II) capture by UNC surface active sites and internal voids [22]. When the concentration of Cd(II) continued to increase, the surface active sites and internal voids of UNC tended to be saturated, and the diffusion rate of Cd(II) slowed down due to the increase of concentration, so that the rate of Cd(II) reaching the surface of UNC slowed down. Therefore, the adsorption capacity decreased slightly. Consequently, when the initial concentration of Cd(II) solution is 900 mg·L<sup>-1</sup>, the adsorption effect is the best.

### 3.2.2 The pH value of the Cd(II) solution

When the initial concentration of Cd(II) solution was 900 mg·L<sup>-1</sup>, the adsorption temperature was 45 °C, and the adsorption time was 2 h, the effect of pH value of Cd(II) solution on the adsorption capacity of Cd(II) adsorbed by UNC was shown in Fig. 4b. From Fig. 4b, it can be seen that the adsorption capacity gradually increases with the decrease of pH value. When pH = 0.89, the adsorption capacity of UNC is the largest, and the adsorption capacity is 606.41 mg·g<sup>-1</sup>. With the increase of pH, the -OH in the solution gradually increased, and Cd(II) and -OH formed a complex [23], which was not conducive to the adsorption of Cd(II) by UNC, so the adsorption capacity gradually decreased. This phenomenon can be explained by Pearson's HSAB theory (hard and soft acid–base theory). According to HSAB theory, Cd(II) is classified as a hard acid. Therefore, Cd(II) has a smaller ionic radius and a higher charge density, which can form strong ionic bonds with hard bases. -OH is classified as hard base. Therefore, in the case of high pH, with the increase of -OH in the solution, Cd(II) is more likely to react with -OH to form stable compounds, resulting in a decrease in adsorption capacity. When the solution is in low acidity, the content of H<sup>+</sup> is high. Due to the high porosity and strong acid and alkali resistance of UNC, Cd(II) is more adsorbed by UNC. Therefore, pH = 0.89 is the best adsorption pH.

### 3.2.3 Adsorption temperature

When the adsorption time was 2 h, the initial concentration of Cd(II) solution was  $900 \text{ mg}\cdot\text{L}^{-1}$ , and the pH was 0.89, the effect of adsorption temperature on the adsorption capacity of UNC for Cd(II) was shown in Fig. 4c. From Fig. 4c, it can be seen that with the increase of adsorption temperature, the adsorption capacity of UNC for Cd(II) increased first and then decreased. When the adsorption temperature was  $45 \text{ }^\circ\text{C}$ , the adsorption capacity reached a maximum of  $610.34 \text{ mg}\cdot\text{g}^{-1}$ . When the temperature is low, the activity of Cd(II) is low, and it cannot fully contact with the adsorption sites and active sites of UNC [24]. When the temperature is too high, the adsorption capacity decreases sharply, which indicates that the temperature has a great influence on the adsorption of Cd(II) by UNC. The increase of temperature will make the internal structure of UNC loose, and the movement of Cd(II) will be intensified [25]. Some Cd(II) will be separated from UNC and the adsorption capacity will be reduced. Therefore, the adsorption effect is the best when the adsorption temperature is  $45 \text{ }^\circ\text{C}$ .

### 3.2.4 Adsorption time

When the initial concentration of Cd(II) solution is  $900 \text{ mg}\cdot\text{L}^{-1}$ , the adsorption temperature is  $45 \text{ }^\circ\text{C}$ , and the pH is 0.89, the effect of adsorption time on the adsorption capacity of UNC for Cd(II) is shown in Fig. 4d. From Fig. 4d, it can be seen that with the increase of adsorption time, the adsorption capacity of UNC for Cd(II) increases first and then decreases. When the adsorption time is 2 h, the adsorption capacity reaches a maximum of  $607.37 \text{ mg}\cdot\text{g}^{-1}$ . With the continuous growth of adsorption time, when the time reaches 2 h, the adsorption of UNC reaches saturation [26]. After the time continues to increase, the adsorption capacity begins to decrease, which is because the adsorption sites continue to decrease, and the electrostatic repulsion continues to increase [27]. In addition, the internal structure of UNC becomes looser due to the increase of adsorption time, resulting in some Cd(II) gradually falling off from UNC. Therefore, 2 h is the best adsorption time.

Through the exploration of the aforementioned four factors, UNC achieved an adsorption capacity of  $611.89 \text{ mg}\cdot\text{g}^{-1}$  for Cd(II) within 2 h. To better understand the performance of UNC, the adsorption performance of this adsorbent is compared with other studies [28, 29]. Table 3 lists some adsorbents used by researchers, and by comprehensive comparison with the different adsorbents listed in Table 3, UNC demonstrates excellent Cd(II) adsorption capability.

### 3.3 Adsorption kinetics

The relationship between adsorption rate and adsorption dynamic equilibrium was analyzed by adsorption kinetics method. In order to further understand the adsorption mechanism of Cd(II) on UNC, the pseudo-first-order and pseudo-second-order kinetic models were used to fit the experimental data, which were Eqs. (2) and (3), respectively.

The pseudo-first-order kinetic model is represented as Eq. (2) [35]:

$$q_t = q_e(1 - e^{-kt}) \quad (2)$$

$q_t$  (min) the amount of drug adsorbed at moment  $t$  ( $\text{mg}\cdot\text{g}^{-1}$ ),  $q_e$  is the amount of drug adsorbed at equilibrium ( $\text{mg}\cdot\text{g}^{-1}$ ), and  $k$  is the rate constant for the quasi-primary kinetic model ( $\text{min}^{-1}$ ).

The pseudo-second-order kinetic model is represented as Eq. (3):

$$q_t = q_e v_0 t / (q_e + v_0 t) \quad (3)$$

$v_0$  ( $\text{mg}\cdot\text{g}^{-1}\cdot\text{min}^{-1}$ ) is the initial adsorption rate of the pseudo-second-order kinetic model ( $\text{mg}\cdot\text{g}^{-1}\cdot\text{min}^{-1}$ ).

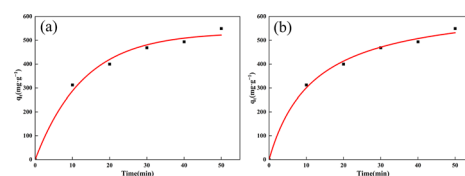


**Fig. 5** The pseudo-first-order (a) and pseudo-second-order (b) kinetic models for the adsorption of Cd(II) by UNC

**Table 3** Comparison of adsorption capacity of different adsorbents

Adsorbent	Initial OTC concentration ( $\text{mg}\cdot\text{L}^{-1}$ )	$q_m$ ( $\text{mg}\cdot\text{g}^{-1}$ )	Time (min)
Clinoptilolite [30]	800	175	60
Fe-montmorillonite [31]	200	50.67	60
HAP-SSBC [32]	300	114.68	60
Hydrochar [33]	50	19.99	60
Vetiver grass biochar (VGB) [34]	100	57.87	100
<b>UNC</b>	<b>900</b>	<b>611.89</b>	<b>120</b>

**Table 4** The pseudo-first-order and pseudo-second-order kinetic parameters of Cd(II) adsorption on UNC

Pseudo-first-order			Pseudo-second-order		
$k$ (min <sup>-1</sup> )	$q_e$ (mg·g <sup>-1</sup> )	$R^2$	$v_o$ (g(mg·min) <sup>-1</sup> )	$q_e$ (mg·g <sup>-1</sup> )	$R^2$
0.073	533.110	0.986	55.191	658.594	0.995

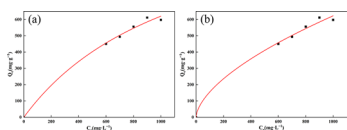

**Fig. 6** Langmuir (a) and Freundlich (b) models of Cd(II) adsorption by UNC

Figure 5 shows the pseudo-first-order (a) and pseudo-second-order (b) kinetic models of UNC adsorbing Cd(II). Table 4 is the pseudo-first-order and pseudo-second-order kinetic parameters of UNC adsorbing Cd(II). According to the parameters in the table, the linear correlation coefficients  $R^2$  of the pseudo-first-order and pseudo-second-order kinetic models of UNC adsorbing Cd(II) are 0.986 and 0.995, respectively, and the theoretical adsorption capacities are 553.110 mg·g<sup>-1</sup> and 658.594 mg·g<sup>-1</sup>, respectively. The actual maximum adsorption capacity of UNC for Cd(II) is 611.89 mg·g<sup>-1</sup>, which has a good linear relationship with the pseudo-second-order kinetics. It can be seen that the adsorption process of Cd(II) by UNC is dominated by chemical adsorption and supplemented by physical adsorption.

### 3.4 Adsorption isotherms

Adsorption isotherms can further describe the adsorption process and adsorption mechanism. The adsorption mechanism of Cd(II) on UNC can be described more accurately by Langmuir and Freundlich isotherm models. They are Eqs. (4) and (5), respectively.

The Langmuir model is represented by Eq. (4) [36]:

$$q_e = q_m C_e / ((1/b) + C_e) \quad (4)$$

$q_e$  is the equilibrium adsorption capacity of OTC (mg·g<sup>-1</sup>),  $q_m$  is the theoretical maximum adsorption capacity (mg·g<sup>-1</sup>) when the surface is completely covered by OTC, and  $b$  is the Langmuir constant (g·mg<sup>-1</sup>).

The Freundlich model is represented by Eq. (5):

$$q_e = K_F C_e^{1/n} \quad (5)$$

$K_F$  (mg<sup>1-1/n</sup>·L<sup>1/n</sup>·g<sup>-1</sup>) is Freundlich constant and  $1/n$  is the adsorption intensity (monolayer adsorption ( $n < 1$ ) and cooperative adsorption ( $n > 1$ )).

**Table 5** The pseudo-first-order and pseudo-second-order kinetic parameters of Cd(II) adsorption on UNC

Langmuir			Freundlich		
$b$ (g·mg <sup>-1</sup> )	$q_e$ (mg·g <sup>-1</sup> )	$R^2$	$K_f$ ((mg·g <sup>-1</sup> ) (L·mg <sup>-1</sup> ) <sup>1/n</sup> )	$1/n$	$R^2$
$8 \times 10^{-3}$	1355.691	0.924	9.705	1.661	0.992

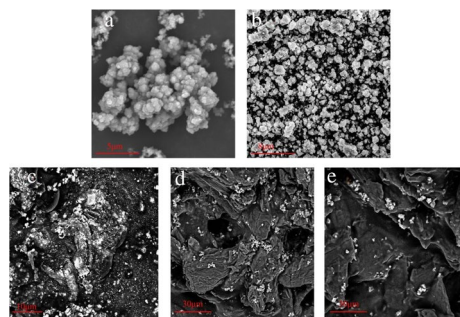

**Fig. 7** SEM photos of UiO-66-NH<sub>2</sub> (a 5 μm, b 8 μm), UiO-66-NH<sub>2</sub> with an added capacity of 0.25 g to UNC (c), UNC (d) before Cd(II) adsorption and UNC (e) after Cd(II) adsorption

Figure 6 shows the Langmuir (a) and Freundlich (b) models of UNC adsorption of Cd(II), and Table 5 presents the Langmuir and Freundlich model parameters for UNC adsorption of Cd(II). According to the data in the table, the linear correlation coefficient ( $R^2$ ) of the Langmuir isotherm model for Cd(II) on UNC is 0.924, with a theoretical adsorption capacity of 1355.691 mg·g<sup>-1</sup>, whereas the actual adsorption capacity is 611.89 mg·g<sup>-1</sup>, indicating a significant deviation from the theoretical value. The Freundlich isotherm model exhibits a good linear correlation, with a coefficient ( $R^2$ ) of 0.992. Therefore, the adsorption process of Cd(II) on UNC is better described by the Freundlich isotherm model, indicating a multilayer adsorption mechanism. Combined with the characterization analysis in Section 3.6.2, it is evident that due to the abundant -OH and -NH<sub>2</sub> groups on the surface and within the pores of UNC, Cd(II) can form coordination bonds with -OH and -NH<sub>2</sub>, leading to its adsorption on both the surface and internal pores of UNC [37]. Additionally, zeta potential experiments revealed that UNC exhibited the maximum negative charge at pH = 0.89, corresponding to the maximum adsorption capacity. At this pH, Cd(II) was also adsorbed via electrostatic interaction, indicating that the adsorption process of Cd(II) by UNC involves multilayer adsorption including both physical and chemical adsorption.

### 3.5 Characterization results and analysis

#### 3.5.1 SEM analysis

Figure 7 (a: 5  $\mu\text{m}$ , b: 8  $\mu\text{m}$ ) is the morphology of UiO-66-NH<sub>2</sub> at 5  $\mu\text{m}$  and 8  $\mu\text{m}$ . Figure 7c–e is the SEM photos of UNC (c) with UiO-66-NH<sub>2</sub> dosage of 0.25 g, UNC (d) before adsorption of Cd(II) and UNC (e) after adsorption of Cd(II). As can be seen from Fig. 7a, b, the SEM image of UiO-66-NH<sub>2</sub> is consistent with the literature description [38]. Due to its inherent agglomeration, it cannot be evenly dispersed, which reduces the number of adsorption sites and active functional groups, and cannot effectively exert its high specific surface area advantage. Figure 7c shows UNC with an added capacity of 0.25 g of UiO-66-NH<sub>2</sub>. From the figure, it can be seen that 0.25 g of UiO-66-NH<sub>2</sub> is agglomerated on the surface of UNC and is too densely distributed. This not only reduces its own number of adsorption sites and active functional groups but also reduces the adsorption sites of cellulose, which seriously affects the adsorption capacity of UNC for Cd(II). Figure 7d is the UNC before adsorption. It can be seen from UNC (d) that UiO-66-NH<sub>2</sub> is loaded in the three-dimensional pores and is evenly distributed. Figure 7e is the UNC after adsorption of Cd(II). SEM photos show that there are still a small number of narrow pores in UNC, but the surface is smooth and flat, which indicates that Cd(II) is successfully adsorbed.

#### 3.5.2 FT-IR analysis

Figure 8 is the FT-IR spectra of UiO-66-NH<sub>2</sub> (a), cellulose (b), UNC (c) before Cd(II) adsorption, and UNC (d) after Cd(II) adsorption. From the FT-IR spectra of UiO-66-NH<sub>2</sub> (a), it can be seen that the adsorption band of 1380–1600  $\text{cm}^{-1}$  is the characteristic adsorption band of UiO-66-NH<sub>2</sub>. Because the ligand of UiO-66-NH<sub>2</sub> is 2-aminoterephthalic acid, it contains aromatic carboxylic acids. Therefore, the peak at 1434  $\text{cm}^{-1}$  is the C–C stretching vibration peak, and the peaks at 1382  $\text{cm}^{-1}$  and 1573  $\text{cm}^{-1}$  are symmetric and asymmetric C–O stretching bonds, respectively, from aromatic and carboxylic acid groups. In

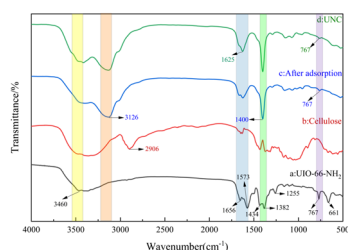


**Fig. 8** FT-IR spectra of UiO-66-NH<sub>2</sub> (a), cellulose (b), UNC after adsorption of Cd(II) (c), and UNC (d)

addition, the C–N stretching vibration peak can be observed at 1255  $\text{cm}^{-1}$ , the peak at 1656  $\text{cm}^{-1}$  is the bending vibration peak of N–H, and the characteristic peaks at 661  $\text{cm}^{-1}$  and 767  $\text{cm}^{-1}$  can be attributed to the Zr–O stretching vibration. These characteristic peaks proved that UiO-66-NH<sub>2</sub> was successfully prepared [39, 40]. From the FT-IR spectra of cellulose (b), it can be seen that the stretching vibration peak of O–H is at 3100–3460  $\text{cm}^{-1}$ , and the absorption peak of C–H is at 2906  $\text{cm}^{-1}$ . However, after the dissolution of cellulose into UNC, the absorption peak at 2906  $\text{cm}^{-1}$  is weakened, which is due to the destruction of the crystal structure of cellulose during dissolution. As evidenced by the FT-IR spectrum of UNC (c) post-adsorption, the O–H stretching vibration peak at 3460  $\text{cm}^{-1}$  weakens following the adsorption of Cd(II), a phenomenon attributed to the reaction between Cd(II) and -OH. The N–H bending vibration peak shifts to a lower wavenumber (1625  $\text{cm}^{-1}$ ), indicative of a chelation reaction between Cd(II) and -NH<sub>2</sub>. Concurrently, Zr–O shifts from a higher to a lower value, underscoring its pivotal role in the adsorption process. These findings are in harmony with the XPS characterization results. As revealed by the FT-IR spectrum of UNC (d) prior to adsorption, the C–H bending vibration peak at 2906  $\text{cm}^{-1}$  in cellulose shifts to a higher wavenumber (3126  $\text{cm}^{-1}$ ). This shift is attributed to the increase in hydrogen bonds during the crosslinking of cellulose with PVA. A characteristic peak of Zr–O emerges at 767  $\text{cm}^{-1}$ , and the stretching vibration peaks at 1400  $\text{cm}^{-1}$ , 1625  $\text{cm}^{-1}$ , and 3460  $\text{cm}^{-1}$  are markedly enhanced. These observations provide compelling evidence that UiO-66-NH<sub>2</sub> has been successfully loaded onto the cellulose.

#### 3.5.3 XRD analysis

Figure 9 shows the XRD patterns of UiO-66-NH<sub>2</sub> (a), cellulose (b) and UNC (c). From the XRD pattern of UiO-66-NH<sub>2</sub> (a), it can be seen that the synthesized UiO-66-NH<sub>2</sub> has a sharp diffraction peak, which indicates that it has excellent crystallinity. UiO-66-NH<sub>2</sub> has obvious crystal plane characteristic diffraction peaks at  $2\theta = 6.8^\circ$ ,  $8.1^\circ$  and  $25.4^\circ$ , and its characteristic diffraction peaks are consistent with those reported in the literature [41], which proves that

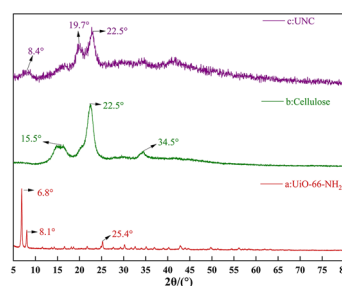


**Fig. 9** XRD patterns of UiO-66-NH<sub>2</sub> (a), cellulose (b), and UNC (c)



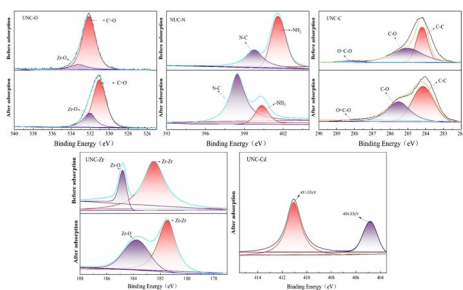


Fig. 10 XPS spectra of UNC before and after adsorption

UiO-66-NH<sub>2</sub> is successfully synthesized. From the XRD patterns of cellulose (b), it can be seen that the (101), (002), and (004) crystal planes of cellulose appeared at  $2\theta = 15.5^\circ$ ,  $22.5^\circ$ , and  $34.5^\circ$ , respectively, which belonged to the characteristics of cellulose crystal type I [42]. According to the XRD spectrum of UNC (c), the characteristic diffraction peak of the crystal plane of the composite film shifted from  $2\theta = 15.5$  to  $19.7^\circ$ , which was due to the deposition of UiO-66-NH<sub>2</sub> in the three-dimensional network structure formed by cellulose and PVA during the blending of UiO-66-NH<sub>2</sub> and cellulose. At the same time, the diffraction peak of regenerated cellulose was weakened, which was due to the crosslinking reaction between cellulose and PVA during the blending process.

### 3.5.4 XPS analysis

Figure 10 shows the XPS spectra of the UNC before and after Cd(II) adsorption. It can be seen from Fig. 10 that the functional groups corresponding to O at 532.13 eV and 533.23 eV in UNC before adsorption are C=O and Zr-O, respectively. After adsorption, C=O and Zr-O shifted ( $532.13 \text{ eV} \rightarrow 531.08 \text{ eV}$  and  $533.23 \text{ eV} \rightarrow 532.03 \text{ eV}$ ), which may be due to the generation of hydrogen bonds and the participation of Zr-O in the adsorption process. The functional groups corresponding to N at 399.78 eV and 401.53 eV in UNC before adsorption were N-C and -NH<sub>2</sub>, respectively [15]. After adsorption, N-C and -NH<sub>2</sub> shifted ( $399.73 \rightarrow 398.43 \text{ eV}$  and  $401.53 \rightarrow 400.33 \text{ eV}$ ), which was due to the chelation reaction between -NH<sub>2</sub> and Cd(II), which was consistent with the results of FT-IR analysis. In the pristine UNC, the functional groups corresponding to the C peaks at 284.18 eV, 285.08 eV, and 288.18 eV are C-C, C-O, and O=C-O, respectively. Upon adsorption, a shift is observed in the C-O peak (from 285.08 to 285.53 eV). This shift is likely attributed to the partial transfer of electron cloud density from the oxygen atom in the C-O group to Cd(II), resulting in the formation of a coordination bond during the adsorption process. The functional groups corresponding to Zr at 184.83 eV and 182.48 eV before adsorption were Zr-O and Zr-Zr,

respectively. After adsorption, both Zr-O and Zr-Zr shifted ( $184.83 \text{ eV} \rightarrow 183.78 \text{ eV}$  and  $182.48 \text{ eV} \rightarrow 181.48 \text{ eV}$ ), indicating that it was involved in the adsorption of Cd(II). The characteristic peaks of Cd appeared at 404.83 eV and 411.03 eV [43, 44], indicating that the successful adsorption of Cd(II) by UNC was consistent with the analysis results of SEM.

### 3.6 Adsorption mechanism

Figure 11 depicts the adsorption mechanism of Cd(II) on the UNC composite membrane. Combined with the analysis results of FT-IR and XPS spectra, it is evident that after Cd(II) adsorption, the FT-IR spectrum of UNC shows a weakening of the stretching vibration peak of O-H at  $3460 \text{ cm}^{-1}$ , and the bending vibration peak of N-H shifts to a lower wavenumber at  $1625 \text{ cm}^{-1}$ . The XPS spectrum displays a shift of the peaks of -NH<sub>2</sub> and Zr-O to lower wavenumbers ( $401.53 \rightarrow 400.33 \text{ eV}$  and  $184.83 \text{ eV} \rightarrow 183.78 \text{ eV}$ ). Thus, O-H, -NH<sub>2</sub>, and Zr-O in UNC all participate in the adsorption process of Cd(II). According to relevant literature, O-H and -NH<sub>2</sub> form coordination bonds with Cd(II), while Zr-O forms a Zr-O-Cd coordination bond [45, 46]. Therefore, the chemical adsorption of Cd(II) on UNC is primarily due to coordination effects. SEM images show that the UNC composite membrane possesses a complex porous structure. During the dissolution and regeneration process, cellulose crosslinks with PVA, forming a three-dimensional network structure. Within the porous network structure, UiO-66-NH<sub>2</sub> is distributed, and Cd(II) is adsorbed inside the material through the pore structure [47]. Through isoelectric point experiments, it is found that the UNC composite membrane exhibits the maximum negative charge at  $\text{pH} = 0.89$ , coinciding with the maximum adsorption capacity. Thus, the physical adsorption of Cd(II) on the UNC composite membrane comprises both electrostatic adsorption and pore filling processes [48]. In summary, the adsorption mechanism of Cd(II) on the UNC composite membrane involves coordination effects, pore filling, and electrostatic interactions.

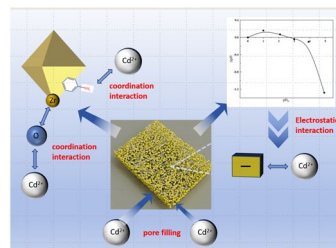
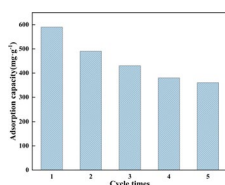


Fig. 11 Adsorption mechanism diagram

Fig. 12 Cyclic adsorption



### 3.7 Cyclic adsorption

Figure 12 shows five cycles of desorption experiments using 4% HNO<sub>3</sub> as the desorbing agent. From the graph, it can be observed that after the first cycle, the adsorption capacity decreased from 611.89 to 580.23 mg g<sup>-1</sup>, resulting in a loss rate of 5%. However, from the second cycle onwards, the reduction in loss rate was approximately 19%, 29%, 37%, and 38%, respectively. The adsorption capacity for the fifth cycle was 381.36 mg g<sup>-1</sup>. Due to the predominantly chemical adsorption of UNC, it is difficult to remove during the desorption process, resulting in the inability of chemical adsorption sites to adsorb again. Moreover, 4% HNO<sub>3</sub> during the desorption process may to some extent damage the membrane material, causing the detachment of UiO-66-NH<sub>2</sub> embedded on the surface and internally. Therefore, the cycling adsorption results show that after five cycles, the adsorption performance of UNC decreased to 381.36 mg g<sup>-1</sup>. However, compared to other types of adsorbents listed in the paper, it still exhibits good adsorption efficiency.

## 4 Conclusion

In summary, the UNC composite membrane was successfully prepared, with UiO-66-NH<sub>2</sub> effectively loaded onto the cellulose nanofilm. Subsequent adsorption experiments revealed that the composite membrane exhibited an adsorption capacity of 611.89 mg·g<sup>-1</sup> for Cd(II), which is superior to other adsorbents listed in the literature. SEM analysis showed that the synthesized UNC composite membrane possessed a complex three-dimensional network structure, originating from the cross-linking of regenerated cellulose and PVA, with UiO-66-NH<sub>2</sub> observed loaded on the surface and within the pores of the composite membrane. FT-IR and XPS analysis of the UNC composite membrane before and after adsorption confirmed that the coordination between Cd(II) and -OH, -NH<sub>2</sub>, and Zr-O was the main driving force for chemical adsorption. Furthermore, combining adsorption kinetics and isotherms further elucidated that the adsorption of Cd(II) by the UNC composite membrane was a complex multilayered adsorption dominated by chemical adsorption with physical adsorption as a supplementary process. Overall, the adsorption mechanism of the UNC composite membrane for Cd(II) involves the coordination between

metal ions and N, O, and pore filling and electrostatic interactions. The UNC composite membrane requires short treatment time, low dosage, and low cost for Cd(II) wastewater treatment, and it also addresses the problem of UiO-66-NH<sub>2</sub> aggregation and pipeline blockage during adsorption. As a membrane material, it has the potential for cyclic adsorption, making it an ideal heavy metal adsorbent.

**Acknowledgements** The authors are sincerely appreciative of School of Materials Science and Art and Design, Inner Mongolia Agricultural University and the authors whose research publications were used for this review work.

**Author contribution** Hao He: investigation, validation, and writing—original draft. Bai-yun Zhao: methodology and conceptualization. Xiao-kai Liu: methodology and conceptualization. Li-juan Zhou: investigation and writing—review. Xuan Zhao: investigation and writing—review. Chen-xu Wang: investigation and writing—review. Li Wang: conceptualization, writing-review and editing, and supervision.

**Funding** This study was supported by the Inner Mongolia Autonomous Region Science and Technology Department Plan Project (2019GG018), the Natural Science Foundation of Inner Mongolia (2021MS02024), and the Inner Mongolia Autonomous Region Science and Technology Department Project (2021GG0213).

**Data availability** Data in all figures are from the experimental results of this experiment.

### Declarations

**Ethics approval** This study is in compliance with ethical standards.

**Consent to participate** All authors agreed with the content.

**Consent for publication** All authors agreed with the content.

**Conflict of interest** The authors declare no competing interests.

## References

- Li YH, Ding J, Luan Z et al (2003) Competitive adsorption of Pb<sup>2+</sup>, Cu<sup>2+</sup> and Cd<sup>2+</sup> ions from aqueous solutions by multiwalled carbon nanotubes[J]. *Carbon* 41(14):2787–2792. [https://doi.org/10.1016/S0008-6223\(03\)00392-0](https://doi.org/10.1016/S0008-6223(03)00392-0)
- Waisberg M, Joseph P, Hale B et al (2003) Molecular and cellular mechanisms of cadmium carcinogenesis[J]. *Toxicology* 192(2–3):95–117. [https://doi.org/10.1016/S0300-483X\(03\)00305-6](https://doi.org/10.1016/S0300-483X(03)00305-6)
- Wang C, Zheng T, Luo R et al (2018) In situ growth of ZIF-8 on PAN fibrous filters for highly efficient U (VI) removal[J]. *ACS Appl Mater Interfaces* 10(28):24164–24171. <https://doi.org/10.1021/acsami.8b07826>
- Hossain MS, Shenashen MA, Awual ME et al (2024) Benign separation, adsorption, and recovery of rare-earth Yb (III) ions with specific ligand-based composite adsorbent[J]. *Process Saf Environ Prot* 185:367–374. <https://doi.org/10.1016/j.psep.2024.03.026>
- Awual ME, Salman MS, Hasan MM et al (2024) Ligand imprinted composite adsorbent for effective Ni (II) ion monitoring and removal from contaminated water[J]. *J Ind Eng Chem* 131:585–592. <https://doi.org/10.1016/j.jiec.2023.10.062>

6. Sheikh MC, Hasan MM, Hasan MN et al (2023) Toxic cadmium (II) monitoring and removal from aqueous solution using ligand-based facial composite adsorbent[J]. *J Mol Liq* 389:122854. <https://doi.org/10.1016/j.molliq.2023.122854>
7. Rasee AI, Awual E, Rehan AI et al (2023) Efficient separation, adsorption, and recovery of Samarium (III) ions using novel ligand-based composite adsorbent[J]. *Surf Interfaces* 41:103276. <https://doi.org/10.1016/j.surfin.2023.103276>
8. Hasan MN, Salman MS, Islam A et al (2021) Sustainable composite sensor material for optical cadmium (II) monitoring and capturing from wastewater[J]. *Microchem J* 161:105800. <https://doi.org/10.1016/j.microc.2020.105800>
9. Dias EM, Petit C (2015) Towards the use of metal–organic frameworks for water reuse: a review of the recent advances in the field of organic pollutants removal and degradation and the next steps in the field[J]. *J Mater Chem A* 3(45):22484–22506. <https://doi.org/10.1039/C5TA05440K>
10. Kumar P, Bansal V, Kim KH et al (2018) Metal-organic frameworks (MOFs) as futuristic options for wastewater treatment[J]. *J Ind Eng Chem* 62:130–145. <https://doi.org/10.1016/j.jiec.2017.12.051>
11. Kumar P, Pournara A, Kim KH et al (2017) Metal-organic frameworks: challenges and opportunities for ion-exchange/sorption applications[J]. *Prog Mater Sci* 86:25–74. <https://doi.org/10.1016/j.pmatsci.2017.01.002>
12. Chen H, Shen C, Chen X et al (2021) High-sensitivity optical fiber hydrogen sensor based on the metal organic frameworks of UiO-66-NH<sub>2</sub>[J]. *Opt Lett* 46(21):5405–5408. <https://doi.org/10.1364/OL.443930>
13. Luu CL, Van Nguyen TT, Nguyen T et al (2015) Synthesis, characterization and adsorption ability of UiO-66-NH<sub>2</sub>[J]. *Adv Natl Sci: Nanosci Nanotechnol* 6(2):025004. <https://doi.org/10.1088/2043-6262/6/2/025004>
14. Sarker M, Song JY, Jhung SH (2018) Carboxylic-acid-functionalized UiO-66-NH<sub>2</sub>: a promising adsorbent for both aqueous-and non-aqueous-phase adsorptions[J]. *Chem Eng J* 331:124–131. <https://doi.org/10.1016/j.cej.2017.08.017>
15. Fang X, Wu S, Wu Y et al (2020) High-efficiency adsorption of norfloxacin using octahedral UiO-66-NH<sub>2</sub> nanomaterials: dynamics, thermodynamics, and mechanisms[J]. *Appl Surf Sci* 518:146226. <https://doi.org/10.1016/j.apsusc.2020.146226>
16. Tian S, Yi Z, Chen J et al (2023) In situ growth of UiO-66-NH<sub>2</sub> in wood-derived cellulose for iodine adsorption[J]. *J Hazard Mater* 443:130236. <https://doi.org/10.1016/j.jhazmat.2022.130236>
17. Zhang Y, Xu X, Yue C et al (2021) Insight into the efficient co-removal of Cr (VI) and Cr (III) by positively charged UiO-66-NH<sub>2</sub> decorated ultrafiltration membrane[J]. *Chem Eng J* 404:126546. <https://doi.org/10.1016/j.cej.2020.126546>
18. Cheng R, Chen Y, Jiang P et al (2023) Deeply removal of trace Cd<sup>2+</sup> from water by bacterial cellulose membrane loaded with nanoscale zerovalent iron: practical application and mechanism[J]. *Chem Eng J* 468:143668. <https://doi.org/10.1016/j.cej.2023.143668>
19. Chen Q, He Q, Lv M et al (2015) Selective adsorption of cationic dyes by UiO-66-NH<sub>2</sub>[J]. *Appl Surf Sci* 327:77–85. <https://doi.org/10.1016/j.apsusc.2014.11.103>
20. Kumar A, Negi YS, Bhardwaj NK et al (2013) Synthesis and characterization of cellulose nanocrystals/PVA based bionanocomposite[J]. *Adv Mater Lett* 4(8):626–631. <https://doi.org/10.5185/amlett.2012.12482>
21. Li X, Tang Y, Xuan Z et al (2007) Study on the preparation of orange peel cellulose adsorbents and biosorption of Cd<sup>2+</sup> from aqueous solution[J]. *Sep Purif Technol* 55(1):69–75. <https://doi.org/10.1016/j.seppur.2006.10.025>
22. Hokkanen S, Repo E, Westholm LJ et al (2014) Adsorption of Ni<sup>2+</sup>, Cd<sup>2+</sup>, PO<sub>4</sub><sup>3-</sup> and NO<sub>3</sub><sup>-</sup> from aqueous solutions by nanostructured microfibrillated cellulose modified with carbonated hydroxyapatite[J]. *Chem Eng J* 252:64–74. <https://doi.org/10.1016/j.cej.2014.04.101>
23. Zhang L, Cai J, Zhou J et al (2005) Adsorption of Cd<sup>2+</sup> and Cu<sup>2+</sup> on ion-exchange beads from cellulose/alginate blend[J]. *Sep Sci Technol* 39(5):1203–1219. <https://doi.org/10.1081/SS-120028579>
24. Awual MR, Hasan MM (2015) Fine-tuning mesoporous adsorbent for simultaneous ultra-trace palladium (II) detection, separation and recovery[J]. *J Ind Eng Chem* 21:507–515. <https://doi.org/10.1016/j.jiec.2014.03.013>
25. Zhang Z, Wang T, Zhang H et al (2021) Adsorption of Pb (II) and Cd (II) by magnetic activated carbon and its mechanism[J]. *Sci Total Environ* 757:143910. <https://doi.org/10.1016/j.scitotenv.2020.143910>
26. Awual MR, Hasan MM, Islam A et al (2019) Offering an innovative composited material for effective lead (II) monitoring and removal from polluted water[J]. *J Clean Prod* 231:214–223. <https://doi.org/10.1016/j.jclepro.2019.05.125>
27. Awual MR (2017) Novel nanocomposite materials for efficient and selective mercury ions capturing from wastewater[J]. *Chem Eng J* 307:456–465. <https://doi.org/10.1016/j.cej.2016.08.108>
28. Ibrahim BM, Fakhre NA (2019) Crown ether modification of starch for adsorption of heavy metals from synthetic wastewater[J]. *Int J Biol Macromol* 123:70–80. <https://doi.org/10.1016/j.ijbiomac.2018.11.058>
29. Fakhre NA, Ibrahim BM (2018) The use of new chemically modified cellulose for heavy metal ion adsorption[J]. *J Hazard Mater* 343:324–331. <https://doi.org/10.1016/j.jhazmat.2017.08.043>
30. Hamoudi SA, Khelifa N, Nouri L et al (2023) Removal of Pb<sup>2+</sup> and Cd<sup>2+</sup> by adsorption onto Y zeolite and its selectivity of retention in an actual contaminated effluent[J]. *Colloid Polym Sci* 301(6):631–645. <https://doi.org/10.1007/s00396-023-05089-y>
31. Wu P, Wu W, Li S et al (2009) Removal of Cd<sup>2+</sup> from aqueous solution by adsorption using Fe-montmorillonite[J]. *J Hazard Mater* 169(1–3):824–830. <https://doi.org/10.1016/j.jhazmat.2009.04.022>
32. Chen Y, Li M, Li Y et al (2021) Hydroxyapatite modified sludge-based biochar for the adsorption of Cu<sup>2+</sup> and Cd<sup>2+</sup>: adsorption behavior and mechanisms[J]. *Biores Technol* 321:124413. <https://doi.org/10.1016/j.biortech.2020.124413>
33. Li D, Cui H, Cheng Y et al (2021) Chemical aging of hydrochar improves the Cd<sup>2+</sup> adsorption capacity from aqueous solution[J]. *Environ Pollut* 287:117562. <https://doi.org/10.1016/j.envpol.2021.117562>
34. Dai W, Xu M, Zhao Z et al (2021) Characteristics and quantification of mechanisms of Cd<sup>2+</sup> adsorption by biochars derived from three different plant-based biomass[J]. *Arab J Chem* 14(5):103119. <https://doi.org/10.1016/j.arabjc.2021.103119>
35. Sharef HY, Jalal AF, Ibrahim BM et al (2023) New ion-imprinted polymer for selective removal of Cu<sup>2+</sup> ion in aqueous solution using extracted Aloe vera leaves as a monomer[J]. *Int J Biol Macromol* 239:124318. <https://doi.org/10.1016/j.ijbiomac.2023.124318>
36. Ibrahim BM, Fakhre NA, Jalhoom MG et al (2022) Removal of lead ions from aqueous solutions by modified cellulose[J]. *Environ Technol* 1–13. <https://doi.org/10.1080/09593330.2022.2056086>
37. Shahat A, Kubra KT, El-marghany A (2023) Equilibrium, thermodynamic and kinetic modeling of triclosan adsorption on mesoporous carbon nanosphere: optimization using Box-Behnken design[J]. *J Mol Liq* 383:122166. <https://doi.org/10.1016/j.molliq.2023.122166>
38. Chen J, Zhang B, Dang X et al (2020) A nanocomposite consisting of etched multiwalled carbon nanotubes, amino-modified metal-organic framework UiO-66 and polyaniline for preconcentration

- of polycyclic aromatic hydrocarbons prior to their determination by HPLC[J]. *Microchim Acta* 187:1–9. <https://doi.org/10.1007/s00604-019-3997-1>
39. Fang Y, Zhang L, Zhao Q et al (2019) Highly selective visible-light photocatalytic benzene hydroxylation to phenol using a new heterogeneous photocatalyst UiO-66-NH<sub>2</sub>-SA-V[J]. *Catal Lett* 149:2408–2414. <https://doi.org/10.1007/s10562-019-02842-3>
40. Zhang X, Zhang Y, Wang T et al (2019) A thin film nanocomposite membrane with pre-immobilized UiO-66-NH<sub>2</sub> toward enhanced nanofiltration performance[J]. *RSC Adv* 9(43):24802–24810. <https://doi.org/10.1039/C9RA04714J>
41. Shen L, Wu W, Liang R et al (2013) Highly dispersed palladium nanoparticles anchored on UiO-66(NH<sub>2</sub>) metal-organic framework as a reusable and dual functional visible-light-driven photocatalyst[J]. *Nanoscale* 5(19):9374–9382. <https://doi.org/10.1039/C3NR03153E>
42. Lu J, Wang T, Drzal LT (2008) Preparation and properties of microfibrillated cellulose polyvinyl alcohol composite materials[J]. *Compos A Appl Sci Manuf* 39(5):738–746. <https://doi.org/10.1016/j.compositesa.2008.02.003>
43. Xie F, Guo J, Wang H et al (2022) Construction of ZnO/CdS/Ag composite photocatalyst and its catalytic and antibacterial performance[J]. *Chinese J Mater Res* 37(1):10–20. <https://doi.org/10.11901/1005.3093.2021.586>
44. Du Z, Yang D, Cao Q et al (2023) Recent advances in catalytic synthesis of 2, 5-furandimethanol from 5-hydroxymethylfurfural and carbohydrates[J]. *Bioresources Bioprocess* 10(1):1–17. <https://doi.org/10.1186/s40643-023-00676-x>
45. Awual MR, Hasan MM, Khaleque MA et al (2016) Treatment of copper (II) containing wastewater by a newly developed ligand based facial conjugate materials[J]. *Chem Eng J* 288:368–376. <https://doi.org/10.1016/j.cej.2015.11.108>
46. Waliullah RM, Rehan AI, Awual ME et al (2023) Optimization of toxic dye removal from contaminated water using chitosan-grafted novel nanocomposite adsorbent[J]. *J Mol Liq* 388:122763. <https://doi.org/10.1016/j.molliq.2023.122763>
47. Hasan MN, Shenashen MA, Hasan MM et al (2021) Assessing of cesium removal from wastewater using functionalized wood cellulose adsorbent[J]. *Chemosphere* 270:128668. <https://doi.org/10.1016/j.chemosphere.2020.128668>
48. Awual MR (2019) A facile composite material for enhanced cadmium (II) ion capturing from wastewater[J]. *J Environ Chem Eng* 7(5):103378. <https://doi.org/10.1016/j.jece.2019.103378>

**Publisher's Note** Springer Nature remains neutral with regard to jurisdictional claims in published maps and institutional affiliations.

Springer Nature or its licensor (e.g. a society or other partner) holds exclusive rights to this article under a publishing agreement with the author(s) or other rightsholder(s); author self-archiving of the accepted manuscript version of this article is solely governed by the terms of such publishing agreement and applicable law.